A New Non-linear Joint Model for RF Energy Harvesters in Wireless Networks

Dokhyl AlQahtani, *Student Member, IEEE,* Yunfei Chen, *Senior Member, IEEE,* Wei Feng, *Senior Member, IEEE,* and Mohamed-Slim Alouini, *Fellow, IEEE*

***Abstract*—Many previous works have treated the conversion efficiency of an energy harvester as a constant or a non-linear function of input power, ignoring the non-linear effect of the operating frequency. Such assumption may lead to erroneous performance analysis or improper resource allocation. In this paper, a novel model is proposed to capture the non-linearity of the conversion efficiency as a function of the frequency and power. The paper first exploits the practical harvesters in the literature to model the conversion efficiency as a function of frequency at fixed power. Based on the shape of the efficiency curve, two categories of harvesters are referred to as Type-I and Type-II. The best-fit model for each category is selected based on the adjusted R-square test. Next, these models are extended to jointly consider both power and frequency dependencies. Using these models, the performances of broad-band simultaneous wireless information and power transfer and OFDM hybrid access point are analysed and optimised. Iterative algorithms are used to find low-complexity solutions. Moreover, the impact of the non-linear conversion efficiency on the average battery life in LoRaWAN is analysed. Our results highlight the significant impact of using the joint model of conversion efficiency.**

***Index Terms*—Conversion efficiency, curve fitting, energy harvesting, wireless communications.**

I. Introduction

ENERGY harvesting has been the focus of many researches that aim to scavenge energy from either the surrounding environment (e.g., sun, heat, motion, radio-frequency (RF), etc.) or a dedicated energy source [1]. The rise of interest in RF energy harvesting is due to its many benefits, including controllable wireless charging to remote devices, no battery replacement, extended node lifetime, and an additional battery in a device [2]. For all works on RF energy harvesting, there is a primary performance metric, namely, the conversion efficiency defined as $\eta = P_{out}/P_{in}$, where P_{out} is the produced direct current (DC) power and P_{in} is the received RF power. The power amplifier non-linearity is included in P_{in}, but this effect is not explicitly discussed in the literature. Most energy harvesting system designs assume that the conversion efficiency is independent of the operating frequency by using a constant model, where the produced DC power is linearly proportional to the input power, or a non-linear model of the input power only. These assumptions are, in general, not accurate, especially when a multi-carrier communications system is considered. In practice, the conversion efficiency is usually a non-linear function of the input power [3]–[6] and the operating frequency [7]–[19]. As a result, the oversimplified model, derived by ignoring the frequency effect, may result in inefficient resource allocation or improper designs for practical communications systems.

There have been quite a few works in the literature on modelling the non-linearity of the conversion efficiency and its effect on resource allocation and wireless communications performance [3]–[6]. However, most of these works focus on the non-linear relationship between the conversion efficiency and the input power. For instance, in [3], the total harvested power as a function of the input RF power was approximated as a logistic (sigmoidal) function to give a non-linear relationship between the conversion efficiency and the input power. Its accuracy can be further improved by considering the harvester sensitivity [20]. Apart from the practicality and accuracy issues, the sigmoidal model might be too complex and mathematically intractable for statistical performance analysis. Hence, the piece-wise linear model for the conversion efficiency was studied in [4], [21]. The piece-wise linear model works remarkably well and offers accuracy proportional to the order of data points used. Note that [21] also used a high-order polynomial in dBm over a range of input power. In addition to the sigmoidal and piece-wise linear models, a rational model was proposed in [5] to achieve both tractability and accuracy by applying curve fitting to experimental data directly. All these models do not directly correspond to a convex function with respect to the input power. Consequently, an optimal solution by introducing pseudo-inverse of the conversion efficiency's non-linear model was derived in [22]. Also, a simpler but less accurate model was proposed as a quadratic function model in [6]. With the convexity property of the quadratic model, the problem of resource allocation using this model directly corresponds to a convex optimisation problem [23]. In order to analyse the energy harvesting systems comprehensively from various perspectives, a multi-objective optimisation method was used

This work was supported in part by EC H2020 DAWN4IoE-Data AwareWireless Network for Internet-of-Everything (778305) and in part by the National Key R&D Program of China under Grant 2020YFA0711301, the National Natural Science Foundation of China (Grant No. 61941104, 61771286), and the Beijing Innovation Center for Future Chip.

Dokhyl AlQahtani is with the School of Engineering, University of Warwick, Coventry, U.K. CV4 7AL. He is also with the Department of Electrical Engineering, Prince Sattam bin Abdulaziz University, Al-Kharj 11942, Saudi Arabia (e-mail:dokhyl.alqahtani@warwick.ac.uk).

Yunfei Chen is with the School of Engineering, University of Warwick, Coventry, U.K. CV4 7AL (e-mail: Yunfei.Chen@warwick.ac.uk).

Wei Feng is with Department of Electronic Engineering, Tsinghua University, Beijing, China (e-mail: fengwei@tsinghua.edu.cn).

Mohamed-Slim Alouini is with the Computer, Electrical, and Mathematical Science and Engineering (CEMSE) Division, King Abdullah University of Science and Technology (KAUST), Thuwal, Makkah Province, Saudi Arabia (e-mail:slim.alouini@kaust.edu.sa).

Corresponding Author: Wei Feng

to optimise energy efficiency and spectral efficiency in [24]. In [25], the authors have proposed a resource management scheme that jointly minimises the transmitted power, maximises the weighted sum of coverage probability of energy harvesting, and minimises the effect of calibration error on the information decoding performance. In [26], time slot duration, transmission power at the source and the relay, and subcarriers for multiple users were jointly considered for orthogonal frequency division multiple access (OFDMA) wireless power transfer (WPT)-assisted relaying systems.

All the above works focus on the dependence of the conversion efficiency on the input power. In practical multi-carrier systems, the conversion efficiency also depends on the frequency and ignoring this will lead to inaccurate performance evaluation and resource allocation. Similarly, the performance of practical maximum power point tracking MPPT-based RF energy harvesting systems may degrade severely with inaccurate models of the dependence of the conversion efficiency on the frequency models. Other research directions in energy harvesting wireless communication are secure WPT by utilising blockchain [27], [28], AC computing [29], and RF Combining [30].

In this work, we propose a joint model for the conversion efficiency that accounts for effects of input power and operating frequency simultaneously to provide a full characterisation of the non-linearity in conversion efficiency. First, new models for the conversion efficiency as a function of the operating frequency that capture the non-linear behaviours of the conversion efficiency in the frequency domain without knowledge of circuit parameters are analysed. Two models are provided as Type-I and Type-II frequency dependency models. Since spectrum and power are the two most important resources in wireless communications, the non-linearity of the conversion efficiency is further investigated as a joint function of input power and operating frequency. The proposed model is essential for many practical applications. We select in this paper three potential applications to show the importance of accurate joint model. The spectral efficiency of broad-band SWIPT in [31] and the OFDM hybrid access point (H-AP) in [32] are investigated and then compared with previous works that have assumed a constant conversion efficiency. Numerical results are presented to show the significant difference between performances predicted using the conventional ideal constant conversion efficiency model and our proposed practical non-linear conversion efficiency model. Also, optimisation problems for these applications are formulated with constraints from the practical limits. Further, to avoid exhaustive searching, an iterative algorithm to solve the optimisation problems with less complexity are provided. Finally, the impact of the non-linearity on the average battery life of a monitoring device in a long-range wide area network (LoRaWAN) in [33] is investigated.

II. Methods of Conversion Efficiency Modelling

The modelling method used in this paper can be decomposed into three main steps. Firstly, experimental data, which show the dependency of the conversion efficiency on the frequency, are copied from different works in the literature. We did not perform any experiments. To avoid overfitting, works from different researchers are used to construct our models. Secondly, the curve fitting technique based on the least-squares method is employed to derive the mathematical model and to choose the best fit among all the models examined. Lastly, the goodness-of-fit, measured by the adjusted R-squared test, is used to verify the model fitness as well as to determine the model order based on an acceptable significance level. These steps are detailed as follows.

A. Literature Review of Experimental Results

The main component of an RF energy harvester is the rectenna, which consists of an antenna and a rectifier. The antenna captures the RF power, and the rectifier converts the captured RF power into DC power. In this subsection, we review different rectenna designs related to our modelling work. For this purpose, they are categorised based on the shape of their curves as Type-I harvester and Type-II harvester. Each type has visual similarities which will be a beneficially utilised in modelling selection. The Type-I harvesters refer to those harvesters that operate at multiple narrow frequency bands separated from each other. This is, for example, the case in the WiFi band where most devices work on both the 2.4GHz and 5.8GHz bands. The Type-II harvesters refer to those harvesters that work over a continuous and large frequency band. This is, for example, the case for the TV band.

Table I reviews the main parameters of the energy harvesters available in the literature, where η_{max} is the maximum achievable efficiency, $f_{\eta_{max}}$ is the frequency that achieves η_{max}, and P_T is the input power that achieves η_{max}. There have been many other works on energy harvester designs in the literature, but the above works are the only works that study the relationship between the conversion efficiency and the operating frequency. Thus, we will focus on these works only.

There are several reasons why modelling conversion efficiency as a function of frequency has important practical uses. For many practical systems, especially multi-carrier communications systems (e.g. OFDM), although the centre frequency is fixed, the actual operating frequency may not be fixed and depends on the allocated subcarrier. From the subcarrier allocation's viewpoint, in many energy harvesting OFDM systems, the subcarriers are often divided into two groups, one group for information decoding and the other group for energy harvesting. Thus, efficient subcarrier allocation in these systems has to take into account the non-linearity of conversion efficiency frequency. Further, maximum power point tracking based RF energy harvesting systems [34] adjust the switching frequency and other operating parameters of a resonant to find the maximum possible power. Therefore, modelling the conversion efficiency as a function of frequency plays an important role for accurate tracking systems. Moreover, practical systems may suffer from frequency offset, such as the Doppler shift and carrier synchronisation error. Our model translates these uncertainties into harvested power changes. The frequency offset can be estimated, but the estimation error is random [35]. Our model can also translate this random estimation error into

TABLE I
MAIN PARAMETERS OF DIFFERENT ENERGY HARVESTERS

Ref.	Type	Operating Bands	η_{max}	$f_{\eta max}$	P_T
[7]	Type-I	2.45 GHz ISM band	38.2%	2.43 GHz	−19.2 dBm
[8]	Type-I	0.75 – 1 GHz	45%	0.9 GHz	−10 dBm
[9]	Type-I	GSM1800 and UMTS-2100 bands	40%	1.84 GHz	−18 dBm
[10]	Type-I	GSM900 and GSM1800	62%	0.88 GHz	0 dBm
[11]	Type-I	2.45 and 5.8 GHz	75%	2.5 GHz	17.7 dBm
[12]	Type-I	ISM bands of 915 MHz and 2.4 GHz	72%	915 MHz	−5 dBm
[13]	Type-I	GSM900, GSM1800, and 3G	55%	0.9 GHz	−10 dBm
[14]	Type-I	0.55, 0.75, 0.9, 1.85, 2.15, and 2.45 GHz	62%	550 MHz	−10 dBm
[15]	Type-II	LTE bands (range 0.79 – 0.96 GHz, 1.71 – 2.17 GHz, and 2.5 – 2.69 GHz)	60%	1 GHz	0 dBm
[16]	Type-II	0.87 – 2.7 GHz	63%	1.1 GHz	0 dBm
[17]	Type-II	450 – 900 MHz	77%	0.68 GHz	−1 dBm
[18]	Type-II	2.3 – 2.85 GHz	68%	2.45 GHz	0 dBm
[19]	Type-II	1.8 – 2.5 GHz	70%	2.15 GHz	−10 dBm

changes in harvested power. Thus, it is important to evaluate the efficiency of harvester in general conditions.

B. Curve Fitting

Curve fitting is a process of specifying a model and then finding the parameters of this model that provide the best fit to a set of N observation pairs, $\{(\bar{x}_i, \bar{y}_i), i = 1, 2, ..., N\}$, where $\bar{y}_i$ is the ith observation at the point $\bar{x}_i$. Let $f(x, \bar{n})$ be a known function of x parametrised in $\bar{n}$, the minimal number of coefficients. Once $\bar{n}$ is known, the function is determined uniquely. Curve fitting aims to find the optimal parameter set $\bar{n}$ using the least squares method by minimizing the square of the error between the measured values y_i and the values determined from the model $f(\bar{x}_i, \bar{n})$. That is, given N measurement pairs $(\bar{x}_i, \bar{y}_i)$, find $\bar{n}$ to minimise [36]:

$$s(\bar{n}) = \sum_{i=1}^{N} (\bar{y}_i - f(\bar{x}_i, \bar{n}))^2 \ . \tag{1}$$

Several curve fitting models are available in MATLAB. Table II shows the main models, their equations and their descriptions, to be used later. We will use curve fitting to propose new models using the experimental data reported in the works discussed in Section II-A.

C. Goodness of Fit

The least-squares method is used to build a model, whereas goodness of fit analysis is used to assess the goodness of the model to the experimental data. We have selected the adjusted R-square test because it has been widely used as the criterion for the quality of fitting [37]. Adjusted R-square adjusts the statistic based on the number of independent variables in the model. Adjusted R-square also indicates how well all the terms fit a curve and adjusts the number of terms in a model. It is defined as:

$$R_{square} = 1 - \frac{(N-1)\sum_{i=1}^{N} w_i \left(y_i - f(\bar{x}_i, \bar{n})\right)^2}{(N-m)\sum_{i=1}^{N} w_i \left(y_i - \hat{y}_i\right)^2}, \tag{2}$$

where w_i is the weighting coefficient applied to each measurement point, usually $w_i = 1$ means that all measurements are equal, $\hat{y}_i = \frac{1}{N}\sum_{i=1}^{N} y_i$ is the mean of the measured values, and m is the number of fitted coefficients of the model. The adjusted R-square statistic can take on any values less than or equal to 1, with a value closer to 1 indicating a better fit. Negative values can also occur when the model contains terms that do not help to predict the response. The adjusted R-square statistic will be used in our fitting work to compare and choose the models.

Complexity of these models is inherently linked to the model order. In order to determine the model order, we will select an acceptable significance level empirically based on the trade-off between the accuracy of the model and its complexity. The acceptable significance level set in this paper is a level of 90% or higher. This gives a good balance between model complexity and accuracy. Other confidence levels are also possible, depending on the requirements for higher accuracy or simpler model. Thus, our method provides flexibility by choosing different model orders for different confidence levels for practical purposes to avoid overfitting, in contrast to methods that only aim for accuracy by using a very high order.

III. NEW MODELS OF CONVERSION EFFICIENCY

This section focuses on modelling the conversion efficiency as a function of frequency. The linear model is motivated by its simplicity rather than its accuracy. Nevertheless, it is the most popular model used in the existing energy harvesting communications literature due to its simplicity. In the literature, the conversion efficiency is typically assumed to be a constant independent of frequency ($0 \leq \eta \leq 1$). However, in practice, the conversion efficiency often changes with the frequency. Next, we will use the experimental data reported in the literature to derive novel non-linear models that fit the conversion efficiency better than the existing linear model.

TABLE II
CURVE FITTING MODELS TESTED

Model	Equation	Description
Weibull	$y = abx^{b-1}e^{-ax^b}$	Weibull Distribution.
Sum of Sine	$y = \sum_{i=1}^{n} (a_i sin(b_i x + c_i))$	Sum of up to eight sine functions.
Rational	$y = \frac{\sum_{i=1}^{n+1} p_i x^{n+1-i}}{x^m + \sum_{i=1}^{m} q_i x^{m-1}}$	Rational models, up to 5th degree/5th degree.
Power	$y = ax^b + c$	Power function.
Gaussian	$y = \sum_{i=1}^{n} a_i e^{\left[-\left(\frac{x-b_i}{c_i}\right)^2\right]}$	Sum of up to eight Gaussian models.
Fourier	$y = a_0 + \sum_{i=1}^{n} (a_i cos(ixw) + b_i sin(ixw))$	Fourier series of up to eight terms.
Exponential	$y = ae^{bx}$	Exponential function and sum of two exponential functions.
Polynomial	$y = \sum_{i=1}^{n+1} p_i x^{n+1-i}$	Polynomial models, up to degree nine.

TABLE III
MODEL COMPARISON BASED ON ADJUSTED R-SQUARE FOR TYPE-I HARVESTER

Ref.	Model							
	Exponential	Fourier	Gaussian	Polynomial	Power	Rational	Sum of Sine	Weibull
[9]	0.1562	0.9313	0.941	0.03114	0.1907	0.3608	0.9308	-3.606
[10]	0.1528	0.8517	0.9737	0.2494	0.06582	0.582	0.8541	0.07811
[11]	-0.05111	0.8634	0.9184	0.7196	-0.03017	0.4312	0.9363	-5.884
[12]	0.06411	0.7689	0.9812	-0.03932	0.02665	0.6427	0.6018	-1.124
[13]	-0.03469	0.3116	0.9414	-0.02374	0.0194	0.4732	0.4539	-0.7093
[14]	-0.05608	0.3568	0.7708	-0.05456	-0.03619	-2.977	0.6276	-2.862

A. Type-I Harvester

The conversion efficiency for Type-I harvester is multi-peak-shaped function. This can be seen in Fig. 1. We have tested exponential, Fourier, Gaussian, polynomial, power, rational, sum of sines, and Weibull models and found that the Gaussian model fits the experimental data best. Table III compares different models in terms of their adjusted R-square values. From Table III, the Gaussian model has the largest adjusted R-square values in most cases. The only exception is for [11], where it has the second largest adjusted R-square value. Considering the balance between accuracy and generality (a general model for all cases), Gaussian is still the best choice. The conversion efficiency η as a non-linear function of frequency for the Type-I harvesters is thus

$$\eta^{\mathrm{NL}}(f) = \sum_{i=1}^{n} a_i e^{\left[-\left(\frac{f-b_i}{c_i}\right)^2\right]}, \tag{3}$$

where f is the frequency in hertz, η^{NL} is the efficiency in percentage, n is the order of the Gaussian model, and the parameters of $a_1, a_2, ..., a_n$, $b_1, b_2, ..., b_n$, and $c_1, c_2, ..., c_n$ are different for different harvesters, which can be determined from the experimental data.

Since Table III shows quantitatively that the Gaussian model is the best choice model for the Type-I harvesters, Fig. 1 compares visually the Gaussian fitted curves with the experimental results for the Type-I harvesters in [9], [10], [13], and [14]. The experimental data are extracted from the figures in these references, whereas the theoretical curves are obtained from the Gaussian model in (3). It should be noted that the visual comparison between models is less accurate compared to the quantitative comparison. So, in our modelling, we mainly use the adjusted R-square for model comparison in Table III and showed the visual comparison of Gaussian model in Fig. 1 for illustration purpose only.

Table IV gives a detailed comparison of different orders of the selected Gaussian model for the goodness of fit based on the adjusted R-square for the Type-I harvesters. As expected, the adjusted R-square values increase as we increase the order of the Gaussian model. However, the improvement becomes marginal beyond a certain threshold. Eventually, the adjusted R-square values become almost identical demonstrating the trade-off between accuracy and complexity. Thus, one is able to maintain accuracy by choosing an acceptable significance level. Another note is that the adjusted R-square for [14] in the last row does not reach 90%. From Table III, the Gaussian model has the largest adjusted R-square value than other models for that harvester. The model type generalisation is still achieved for the Gaussian model for all cases in Type-I harvesters. On the other hand, the adjusted R-square usually increases as the order of the Gaussian model increases. This implies that in the six band case (6 peaks), an order higher than 8 will be needed to reach 90%, but MATLAB has limited capability in this situation. Finally, the fitting parameters for different harvesters discussed in this subsection are listed in Table V based on the orders chosen in Table IV.

B. Type-II Harvester

For Type-II harvesters, we have tested and compared the exponential, Fourier, Gaussian, polynomial, power, rational,

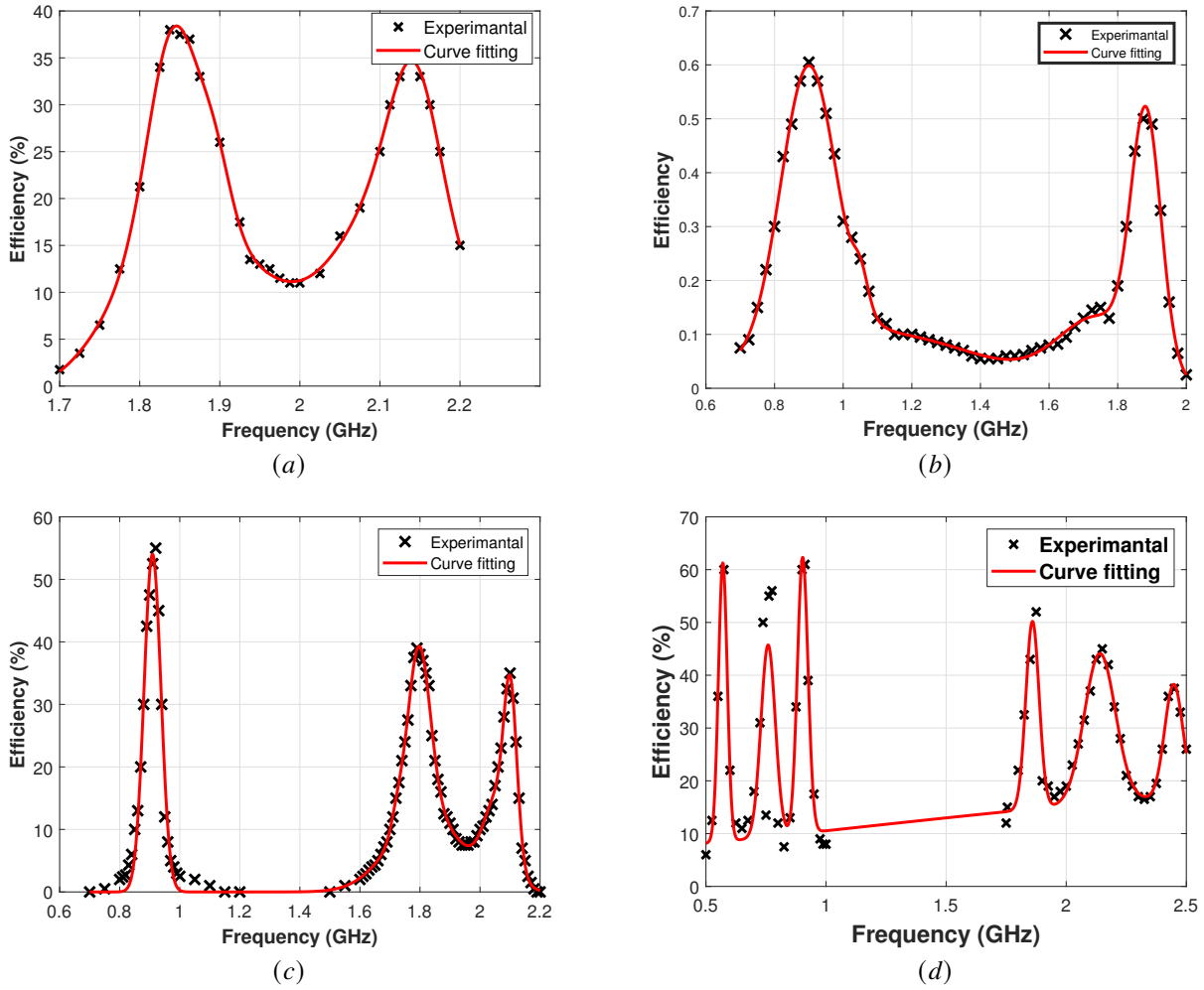

Fig. 1. Comparison of the fitted curve and the experimental data in (a) [9]. P_{in} = −18 dBm (b) [10]. P_{in} = 0 dBm (c) [13]. P_{in} = −10 dBm (d) [14] P_{in} = −10 dBm, for Type-I harvesters.

sum of sines, and Weibull models in terms of their adjusted R-square values as shown in Table VI. We have found that the Fourier model has the largest adjusted R-square values among all models in all cases. Thus, the conversion efficiency η as a non-linear function of frequency for Type-II harvesters is given by

$$\eta^{\mathrm{NL}}(f) = a_0 + \sum_{i=1}^{n} \left(a_i cos(ifw) + b_i sin(ifw)\right), \qquad (4)$$

where $a_0, a_2, ..., a_n$, $b_1, b_2, ..., b_n$, and w are the parameters to be fit for different harvesters. Fig. 2 shows the visual comparison of the experimental results provided in [16], [17], [18], and [19] with the corresponding fitted models for illustration purpose only. Based on the adjusted R-square test for the goodness of fit, Table VII compares different orders of the chosen Fourier model for Type-II harvesters. Again, the goodness of fit improves with the model order but the gain becomes marginal when it reaches a certain threshold to balance complexity and accuracy properly. In Table VIII, we provide the fitting parameters for the Type-II harvesters previously mentioned according to the model orders selected in Table VII. The harvester in [16] has large parameters in this table, which may be caused by its large flat area requiring large factors for sine functions. It is noted that for some harvesters, such as [16], the energy harvesting frequency band could be selected to lie within a linear region. Also, in many passive noise-limited energy harvesting devices, the impact of bandwidth on conversion efficiency can be small due to their large operating bandwidth (tens of MHz). However, the conversion efficiency is determined by both the bandwidth and the centre frequency of the band so that our model will be needed. Also, in practice, due to the frequency offset incurred by the wireless channel, such as the Doppler shift, it may be hard to know what exactly the frequency of the received signal is or it may be desirable for the system to operate on the whole frequency band. Hence, it is useful to have a non-linear model covering all possible frequencies.

IV. Joint Model of Input Power and Operating Frequency

The operating frequency and the input power are two most important resources to be jointly considered in wireless

TABLE IV
GOODNESS OF FIT FOR DIFFERENT ORDERS OF GAUSSIAN MODEL IN TYPE-I HARVESTERS

Ref.	Selected Order	Order							
		1	2	3	4	5	6	7	8
[9]	2	0.01595	0.941	0.9322	0.9686	0.9926	0.9961	0.9947	0.9866
[10]	3	0.1634	0.8517	0.9737	0.9763	0.9703	0.9949	0.9942	0.968
[11]	5	-0.9875	0.6877	0.7937	0.8778	0.9184	0.9243	0.9267	0.9265
[12]	3	-0.2238	0.8953	0.9812	0.9771	0.9974	0.995	0.9966	0.9964
[13]	3	-0.3145	0.5296	0.9414	0.9761	0.9751	0.9829	0.985	0.9838
[14]	7	-0.03614	-0.05709	0.1984	0.2633	0.06441	0.7091	0.7708	0.6588

TABLE V
FITTING PARAMETERS OF THE GAUSSIAN MODELS FOR TYPE-I HARVESTERS

Parameters	Ref.					
	[9]	[10]	[11]	[12]	[13]	[14]
a_1	36.67	0.5321	73.59	46.44	54.02	52.3
b_1	1.856	0.9035	2.438	0.9346	0.9093	0.9029
c_1	0.08455	0.126	0.3244	0.1201	0.03964	0.03111
a_2	31.32	0.4484	49.22	30.84	35.07	52.83
b_2	2.13	1.877	2.855	2.417	1.799	0.5704
c_2	0.1024	0.0627	0.1897	0.3383	0.09177	0.02571
a_3	-	0.08762	63.2	8.308	29.77	36.39
b_3	-	1.501	5.731	1.457	2.085	0.7588
c_3	-	0.8531	0.3478	0.6931	0.05927	0.04216
a_4	-	-	44.47	-	-	35.57
b_4	-	-	2.062	-	-	1.859
c_4	-	-	0.1085	-	-	0.03906
a_5	-	-	57.61	-	-	28.34
b_5	-	-	3.243	-	-	2.14
c_5	-	-	0.2035	-	-	0.09133
a_6	-	-	-	-	-	21.43
b_6	-	-	-	-	-	2.448
c_6	-	-	-	-	-	0.0535
a_7	-	-	-	-	-	18.35
b_7	-	-	-	-	-	3.378
c_7	-	-	-	-	-	3.193

TABLE VI
MODEL COMPARISON BASED ON ADJUSTED R-SQUARE FOR TYPE-II HARVESTER

Ref.	Model							
	Exponential	Fourier	Gaussian	Polynomial	Power	Rational	Sum of Sine	Weibull
[16]	0.6497	0.9071	0.8261	0.5133	0.1442	0.6902	0.8986	-10.19
[17]	0.6583	0.9058	0.895	0.8124	0.5419	0.8099	0.9053	-2.358
[18]	-0.001176	0.98	0.9793	0.01801	-0.01942	-0.03655	0.9108	-4.944
[19]	0.6289	0.9221	0.9035	0.8263	0.3368	0.8605	0.8559	-1.541

TABLE VII
GOODNESS OF FIT FOR DIFFERENT ORDERS OF FOURIER MODEL IN TYPE-II HARVESTERS

Ref.	Selected Order	Order							
		1	2	3	4	5	6	7	8
[16]	2	0.3742	0.9071	0.9442	0.9839	0.9909	0.995	0.9967	0.9988
[17]	2	0.8336	0.9058	0.915	0.9769	0.9779	0.9885	0.9886	0.9925
[18]	1	0.98	0.9866	0.994	0.9929	0.996	0.9968	0.9962	0.9962
[19]	3	0.8744	0.8692	0.9221	0.9614	0.9886	0.9885	0.9941	0.9945

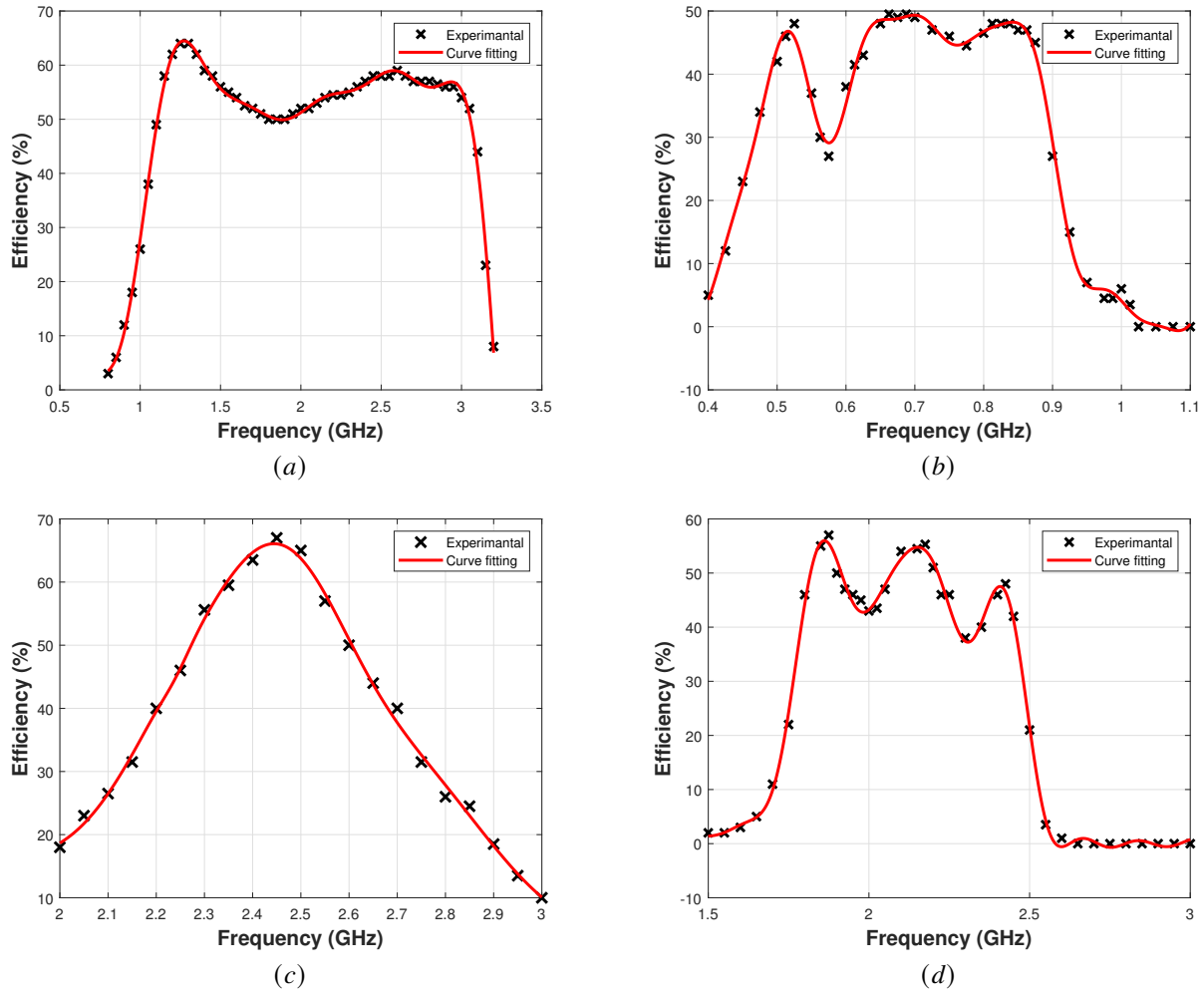

Fig. 2. Comparison of the fitted curve and the experimental data for Type-II harvesters in (a) [16]. P_{in} = 0 dBm. (b) [17]. P_{in} = −1 dBm. (c) [18]. P_{in} = 0 dBm. (d) [19]. P_{in} = −10 dBm.

TABLE VIII
FITTING PARAMETERS OF FOURIER MODEL FOR DIFFERENT TYPE-II HARVESTERS

Ref.	Order	Parameters							
		a_0	a_1	b_1	a_2	b_2	a_3	b_3	w
[16]	2	-1.097e+04	9882	1.113e+04	455.2	-3834	-	-	0.414
[17]	2	29.49	23.16	-6.439	-3.96	7.581	-	-	8.637
[18]	1	38.31	-7.833	23.59	-	-	-	-	5.91
[19]	3	24.71	-25.03	15.67	-0.09291	0.7813	-0.2589	-7.447	4.203

communications. Thus, it is also of great interest to model the non-linearity of the conversion efficiency as a function of both frequency and power. The works in [3]–[6] modelled the conversion efficiency as a function of input power for fixed operating frequencies. Also, in our analytical models above, the conversion efficiency is modelled as a function of the operating frequency for fixed input power. The separate modelling of the input power dependency and the operating frequency dependency may not fully discover the non-linearity of the conversion efficiency. A joint model will be useful to exploit at best the advantage of non-linearity in the conversion efficiency.

The results in [10], [17], [38]–[41] provide the conversion efficiency versus frequency at different input power levels and the conversion efficiency versus input power at different frequencies. This gives

$$\eta_f^{\mathrm{NL}}(f_r, P_u) = \frac{\eta_P^{\mathrm{NL}}(P_u, f_r)}{\eta_P^{\mathrm{NL}}(P_r, f_r)} \eta_f^{\mathrm{NL}}(f_r, P_r), \tag{5}$$

where $\eta_f^{\mathrm{NL}}(f_r, P_u)$ is the conversion efficiency at frequency f_r and input power P_u calculated from the frequency dependency model, $\eta_f^{\mathrm{NL}}(f_r, P_r)$ is the conversion efficiency at frequency f_r

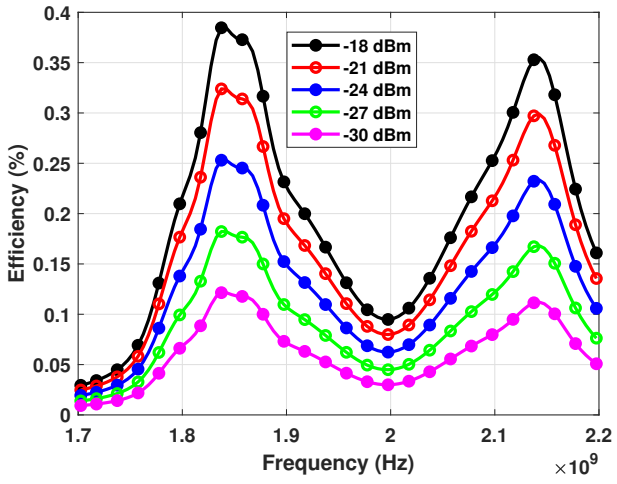

Fig. 3. Measured efficiencies of the rectifier against frequency at different input power levels. Figure reproduced from Ref. [9].

and input power P_r calculated from the frequency dependency model, $\eta_P^{\mathrm{NL}}(P_u, f_r)$ is the conversion efficiency at frequency f_r and input power P_u calculated from the input power dependency model, and $\eta_P^{\mathrm{NL}}(P_r, f_r)$ is the conversion efficiency at frequency f_r and input power P_r calculated from the input power dependency model. For a general value of $P_u = P^{in}$, this becomes

$$\eta_f^{\mathrm{NL}}(f_r, P^{in}) = \frac{\eta_P^{\mathrm{NL}}(P^{in}, f_r)}{\eta_P^{\mathrm{NL}}(P_r, f_r)} \eta_f^{\mathrm{NL}}(f_r, P_r). \tag{6}$$

We have tested the power dependency part of the ratio $\frac{\eta_P^{\mathrm{NL}}(P^{in}, f_r)}{\eta_P^{\mathrm{NL}}(P_r, f_r)}$ at different values of $P_r = 0, -5, -10$ dBm, $P_u = -5, -10, -20$, and different values of $f_r = 0.89, 1.88$ GHz for [10], $f_r = 0.68, 0.85$ GHz for [17], and $f_r = 0.9, 1.8, 2.45$ GHz for [38]. It can be shown that this ratio is approximately independent of f_r and only dependent of P_r and P^{in}. Then this ratio is assumed independent of frequency f_r as $\frac{\eta_P^{\mathrm{NL}}(P^{in})}{\eta_P^{\mathrm{NL}}(P_r)}$. Hence, (6) becomes

$$\eta_f^{\mathrm{NL}}(f, P^{in}) = \frac{\eta_P^{\mathrm{NL}}(P^{in})}{\eta_P^{\mathrm{NL}}(P_r)} \eta_f^{\mathrm{NL}}(f, P_r). \tag{7}$$

Based on that, a general joint model of the non-linear conversion efficiency as a function of both input power and operating frequency is

$$\eta^{\mathrm{NL}}(P^{in}, f) = \frac{1}{\eta_P^{\mathrm{NL}}(P_r)} \eta_P^{\mathrm{NL}}(P^{in}) \eta_f^{\mathrm{NL}}(f), \tag{8}$$

where $\eta_P^{\mathrm{NL}}(P^{in})$ is the conversion efficiency as a function of input power, $\eta_f^{\mathrm{NL}}(f)$ is the conversion efficiency as a function of frequency, and $\eta_P^{\mathrm{NL}}(P_r)$ is the value of the conversion efficiency at P_r calculated from the model of the conversion efficiency as a function of input power with fixed operating frequency at f_r. Fig. 3 shows this relation graphically, emphasizing that the conversion efficiency varying with both frequency and input power.

It is worth noting that our joint model is important for the design of energy harvesting transceivers for the following reasons. It is very difficult to get a full picture of the conversion efficiency experimentally that cover all ranges of operation in the power domain and the frequency domain simultaneously. Thus, the joint model will be helpful to predict the conversion efficiency at any power or frequency of operation without exhaustive experiments. The received RF power is usually unpredictable due to fading and noise. Thus, the conversion efficiency is sensitive to the input power. For the frequency, even the bandwidth is known, the carrier frequency may drift due to Doppler shift etc. so that the overall frequency is also unpredictable and it is important to model the frequency dependence of the conversion efficiency. Otherwise, the frequency dependent models are better suited to cases where the variation of the received RF power is small for some period of time.

V. Applications in Wireless Communications

In this section, the effect of the non-linearity of conversion efficiency as a function of both frequency and power will be investigated for different communications systems. In particular, we consider broad-band SWIPT proposed in [31], OFDM hybrid access point (H-AP) studied in [32], and energy harvesting in LoRaWAN studied in [33]. The fading coefficients are modelled as independent and identically distributed (i.i.d.) complex Gaussian random variables with zero-mean and unit variance throughout the numerical examples. The noises are also i.i.d. complex Gaussian random variables with zero-mean. In the modern communication systems, broad-band rectenna (the bandwidth of more than 1 GHz) is greatly preferred to simultaneously harvest power from multiple frequency bands [42].

A. Broad-band SWIPT

We consider the same system as that in [31] but use the proposed joint model of the non-linear conversion efficiency for comparison. In this case, a base station (BS) communicates with and supplies power to a single user mobile, which sends the information back to the BS using the harvested power. In order to support the full-duplex operation of the information and power transfer, the antenna array at the BS are divided into two sub-arrays, one of which is used to transmit the power to the mobile, and the other is used to receive the information from the mobile. Similarly, the antenna array at the mobile are divided into two sub-arrays, one of which is used to harvest the power, and the other is used to transmit the information to the BS in the uplink. We assume that SWIPT uses a wide frequency band partitioned into K sub-channels. Denote h_k as the downlink channel power from the BS to the mobile over sub-channel k and g_k as the uplink channel power from the mobile to the BS over sub-channel k. Then, the total harvested power by the mobile is given by

$$E_h = \sum_{k=1}^{K} \eta^{\mathrm{NL}}(P_k^{in}, f_k) P_k h_k, \tag{9}$$

where P_k is the downlink transmission power allocated the sub-channel k and P_k^{in} is the received power at the subcarrier k defined as $P_k^{in} = P_k h_k$. The harvested power is used for

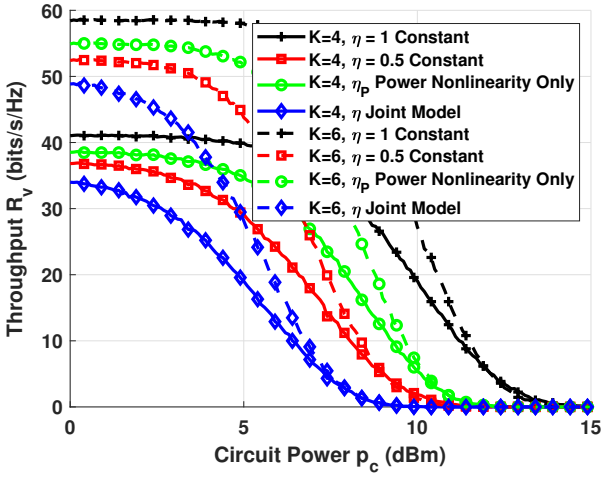

Fig. 4. Constant and non-linear efficiency used to calculate the throughput of broad-band SWIPT as a function of transmitted power for different numbers of subcarriers 4 and 6.

uplink transmission from the mobile to the BS. Subsequently, the uplink throughput, denoted as R_v, was given as [31]

$$R_v = \left[\sum_{k=1}^{K} \log_2\left(1 + \frac{Q_k g_k}{\sigma^2}\right)\right] I\left(E_h \geq p_c\right) \tag{10}$$

where Q_k is the transmission power allocated to sub-channel k in the uplink, and the indicator function $I(\mathcal{E})$ gives 1 if the event $\mathcal{E}$ occurs and 0 otherwise. The indicator function in (10) represents the circuit power constraint required to switch on the user node with a minimum power of p_c or the wake-up power. This power is determined by the sensitivity of the harvester and limits the operation time of the harvester [21]. Energy outage occurs when the input power is below this threshold, as in (10) from the indicator function. However, the study of this threshold is beyond the scope of this work.

In [31], $\eta^{\mathrm{NL}}(P_k^{in}, f_k)$ was assumed constant and independent of the frequency and input power. However, in our model, $\eta^{\mathrm{NL}}(P_k^{in}, f_k)$ depends on both the frequency and the input power. Fig. 4 compares the uplink throughput using the conventional constant efficiency model and our non-linear joint power and frequency dependent efficiency model versus p_c. We assume the use of the harvester in [10]. In this figure, the circuit power p_c changes from 0 dBm to 15 dBm for $K = 4$ and $K = 6$, which is used here to observe if the conversion efficiency changes with value of the operating frequency. Other values can be used too but are not provided here due to limited space. The noise variance is $\sigma^2 = -30$ dBm. The frequency gap between two subcarriers is $\Delta f = B/N$ with $B = 200$ MHz and centre frequency of 1.88 GHz. Note that the total transmission power is $P_T = 10$ dBm, and the experimental transmission power is $P_r = 0$ dBm. For the conventional model, we assume $\eta^{\mathrm{NL}}(P_k^{in}, f_k) = \eta = 1$ and $\eta^{\mathrm{NL}}(P_k^{in}, f_k) = \eta = 0.5$. For the power dependency model, we employ the model proposed in [6]. The throughput reduces with increasing circuit power. As expected, the linear model with $\eta = 1$, the linear model with $\eta = 0.5$, the non-linear power-only model considerably overestimate the throughput performance. Since the linear model overestimates conversion efficiency, it is also overestimating the performance of the system when used. If we use the linear model, our expected value will be larger than the actual value in reality predicted by our model. This shows the usefulness of our model.

B. OFDM Hybrid Access Point (H-AP)

In this example, a hybrid access point broadcasts energy to K users in the downlink, and these users transmit information signals to the H-AP in the uplink using OFDMA through the assigned subcarriers $S(k)$ and they use up all the harvested energy. Consider the same system in [32], where the total bandwidth is equally divided into $N = 4$ subcarriers. The subcarrier scheduling is given by $S(1) = \{3\}$ and $S(2) = \{1, 2, 4\}$. Then, the achievable rate of user k can be expressed as [32]

$$R_k = \sum_{m \in S(k)} \log\left(1 + \frac{h_{U,k}[m] P_{U,k}[m]}{\sigma^2}\right) \times I\left(\sum_{m \notin S(k)} \eta^{\mathrm{NL}}(P_{k,m}^{in}, f_m) P_D[m] h_{D,k}[m] \geq p_c\right), \tag{11}$$

where $h_{U,k}[m]$ and $h_{D,k}[m]$ are fading powers at subcarrier m of user k for uplink and downlink, respectively, $P_{U,k}[m]$ and $P_D[m]$ are the transmit powers at subcarrier m of user k for uplink and downlink, respectively, σ^2 is the noise variance at the user node, $P_{k,m}^{in}$ is the received RF power at subcarrier m of user k defined as $P_{k,m}^{in} = P_D[m] h_{D,k}[m]$, and $\eta^{\mathrm{NL}}(P_{k,m}^{in}, f_m)$ is the conversion efficiency which is assumed constant and independent of the frequency and input power in [32] but in our model, is a non-linear function of both the frequency and input power. Fig. 5 compares the achievable rate of each user using the conventional constant efficiency model and our joint non-linear model. In this comparison, we employed the energy harvester in [10], and for the conventional model, we considered $\eta^{\mathrm{NL}}(P_{k,m}^{in}, f_m) = \eta = 1$ and $\eta^{\mathrm{NL}}(P_{k,m}^{in}, f_m) = \eta = 0.5$. In addition, we employ the model proposed in [6] for the power dependency model. Note that the frequency separation between two subcarriers is $\Delta f = B/N$ with $B = 200$ MHz and centre frequency of 1.88 GHz. The noise variance is $\sigma^2 = -30$ dBm and the total transmitted power is $P_T = 10$ dBm.

Several observations can be made. Firstly, the achievable rate for user 1 is smaller than that for user 2 when the circuit power is low. This is because more uplink subcarriers are allocated to user 2 than to user 1. Secondly, it is evident from this figure that the effect of non-linear frequency dependency model is very clear for user 1 (the size of the gap between curves). This is because user 1 has more downlink subcarriers which suffer from the non-linearity in the frequency domain compared to the user 2, which has only one downlink subcarrier. Finally, user 1 has larger immunity against change in the circuit power than user 2, as user 1 has the probability of harvesting more power than user 2 by having more downlink subcarriers.

C. Optimal Subcarrier And Power Allocation

This section considers a joint subcarrier scheduling and power allocation problem for the OFDM hybrid access point

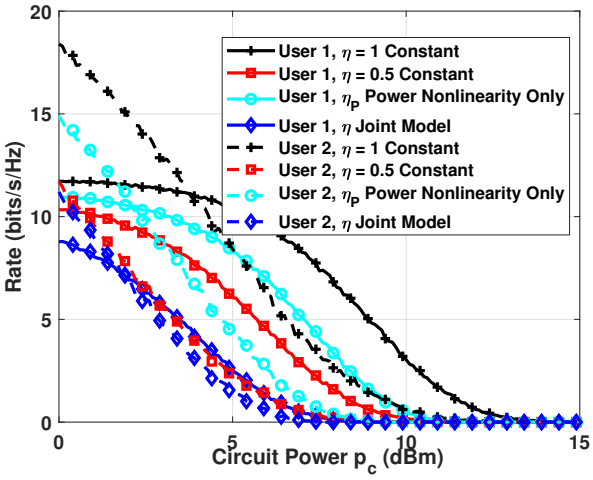

Fig. 5. The achievable rate for each user comparison between constant and non-linear efficiency.

system discussed above. The optimisation problem is formulated first. Then, we propose the optimal resource allocation algorithm to solve the problem efficiently. The optimisation problem to maximise the sum-rate is given by

$$(\mathbb{P}_0): \{\mathcal{S}^*, \mathcal{P}_{\mathcal{D}}{}^*, \mathcal{P}_{\mathcal{U}}{}^*\} = \max_{\{S_k\},\{P_D[m]\},\{P_{U,k}[m]\}} \sum_{k=1}^{K} R_k \tag{12a}$$

$$\text{subject to:} \quad \sum_{m=1}^{N} P_D[m] \le P_T, \tag{12b}$$

$$0 \le P_D[m] \le P_{peak}, \quad \forall m, \tag{12c}$$

$$\sum_{m\in S(k)} P_{U,k}[m] \le \sum_{m\notin S(k)} \eta^{\mathrm{NL}}(P^{in}_{k,m}, f_m) P_D[m] h_{D,k}[m], \quad \forall k, \tag{12d, 12e}$$

where (12b) and (12c) are the total and peak power constraints at the H-AP, respectively, and (12e) makes sure that the total uplink power is not more than the harvested power.

The Problem ($\mathbb{P}_0$) is a mixed-integer non-linear programming (MINLP) problem, which is known to be *NP*-hard, due to the presence of integer subcarrier allocation variables and the coupling of optimisation variables. As a result, an exhaustive search method would be required to solve this problem. To solve the problem efficiently, we need to decouple the subcarrier allocation and power allocation, similar to the approach in [43]. Hence, Problem $\mathbb{P}_0$ can be reformulated as

$$(\mathbb{P}_1): \quad \{\mathcal{S}^*\} = \max_{\{S_k\}} \sum_{k=1}^{K} R_k \tag{13}$$

and

$$(\mathbb{P}_2): \quad \{\mathcal{P}_{\mathcal{D}}{}^*, \mathcal{P}_{\mathcal{U}}{}^*\} = \max_{\{P_D[m]\},\{P_{U,k}[m]\}} \{\sum_{k=1}^{K} R_k | \mathcal{S}^*\} \tag{14a}$$

$$\text{subject to:} \quad (12b) - (12e),$$

which indicate that the subcarrier and power allocation are carried out separately.

Problem ($\mathbb{P}_3$) is generally a nonconvex function due to the coupling of optimisation variables. To derive an efficient power allocation algorithm, we decompose Problem ($\mathbb{P}_3$) into two sub-problems as:

$$(\mathbb{P}_{3A}): \{\mathcal{P}_{\mathcal{D}}{}^*\} = \max_{\{P_D[m]\}} \{\sum_{k=1}^{K} \sum_{m\notin S(k)} \eta^{\mathrm{NL}}(P^{in}_{k,m}, f_m) P_D[m] h_{D,k}[m] | \mathcal{S}^*\} \tag{15a}$$

$$\text{subject to:} \quad (12b) - (12c),$$

and

$$(\mathbb{P}_{3B}): \quad \{\mathcal{P}_{\mathcal{U}}{}^*\} = \max_{\{P_{U,k}[m]\}} \{\sum_{k=1}^{K} R_k | \mathcal{S}^*, \mathcal{P}_{\mathcal{D}}{}^*\} \tag{16a}$$

$$\text{subject to:} \quad (12e).$$

By exploiting the convexity property of the quadratic model in [6], Problems ($\mathbb{P}_{3A}$) and ($\mathbb{P}_{3B}$) are convex optimisation problems that can be efficiently solved by CVX [44]. Therefore, we propose the optimal resource allocation, given by Algorithm 1, which can find the optimal resource allocation for Problem ($\mathbb{P}_0$).

Algorithm 1 Optimal Resource Allocation Algorithm

Subcarrier searching: Find all possible subcarrier combinations which are included in $\mathcal{S}^{(n)}, n = 1, \cdots, N_{perm}$

1: **for** $n = 1, ..., N_{perm}$ **do**
2: Solve the optimisation problem ($\mathbb{P}_{3A}$) by using CVX based on the subcarrier allocation of $\mathcal{S}^{(n)}$.
3: Solve the optimisation problem ($\mathbb{P}_{3B}$) by using CVX based on the subcarrier allocation and the downlink power allocation of $\{\mathcal{S}^{(n)}, \mathcal{P}_{\mathcal{D}}{}^{(n)}\}$.
4: **end for**

Output: the optimal resource allocation result $\{\mathcal{S}^*, \mathcal{P}_{\mathcal{D}}{}^*, \mathcal{P}_{\mathcal{U}}{}^*\} = \max_{\{n=1,\cdots,N_{perm}\}} \{\sum_{k=1}^{K} R_k(\mathcal{S}^{(n)}, \mathcal{P}_{\mathcal{D}}{}^{(n)}, \mathcal{P}_{\mathcal{U}}{}^{(n)})\}$.

Note that any non-linear power model can be incorporated with our proposed algorithm, and the optimal solution of Problem ($\mathbb{P}_{3A}$) can be obtained either by the traditional convex optimisation or by an iterative method such as [22]. Optimising Application 1 can be solved almost identically to the solving Problem ($\mathbb{P}_2$), so we do not repeat here.

Fig. 6 compares the achievable sum-rate obtained from the optimised resource allocation and that from the static allocation technique (equal power and subcarrier allocation) for Application 1 and 2. Also, we compare the proposed Algorithm 1 with the exhaustive search method to verify its

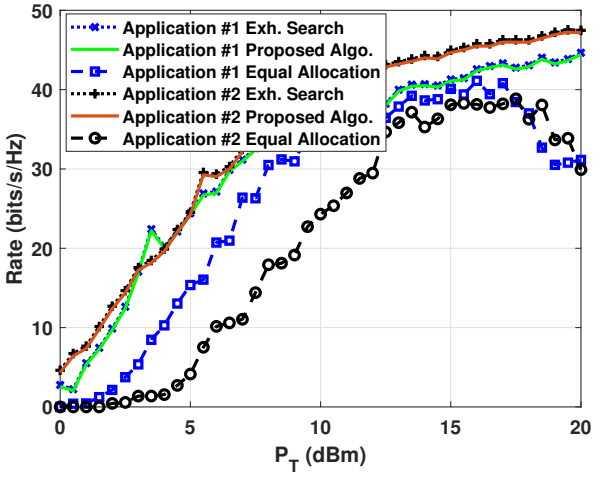

Fig. 6. Average sum-rate versus transmission power for constant and non-linear efficiency.

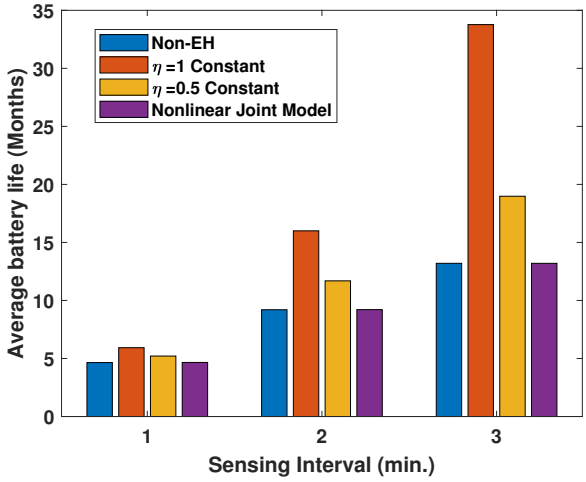

Fig. 7. Average battery life of monitoring device considering different EH conversion efficiency models against sensing interval in LoRaWAN.

optimality. Other parameters are the same as those in Fig. 4 for Application 1, Fig. 5 for Application 2, and $P_{peak} = \frac{P_T}{2}$. As shown in Fig. 6, our proposed algorithm approaches the exhaustive search algorithm with much lower complexity. It can also be seen that the proposed optimisation significantly improves the sum-rate performance over the equal resource allocation scheme for both applications. Finally, due to the harvester circuit saturation effects, the rate decreases for high transmission power for the equal resources allocation.

1) Complexity Analysis: In this part, we analyse the computational complexities of the proposed Algorithm 1 and the exhaustive search. We consider the worst case complexity in terms of the number of comparisons required by each algorithm. For comparison purposes only, we use a fixed step size in the downlink and uplink power allocation problem as Δ. The dimension of the problem $(\mathbb{P}_0)$ is $D = N \times \frac{P_T}{\Delta} \times \frac{P_{peak}}{\Delta}$. Therefore, exhaustive search algorithm requires at most $O(\beta^D)$, and its complexity is exponential with the dimension of the problem. Let us now analyse the complexity of Algorithm 1. We note that due to convexity, problems $(\mathbb{P}_{3A})$ and $(\mathbb{P}_{3B})$ can be solved in polynomial time $O((\frac{P_T}{\Delta})^{\alpha} + (\frac{P_{peak}}{\Delta})^{\alpha})$. In Line 1 of Algorithm 1, the complexity of the subcarrier allocations problem is at most $O(\beta^N)$. Therefore, Algorithm 1 requires at most $O\left(\beta^N \times \left((\frac{P_T}{\Delta})^{\alpha} + (\frac{P_{peak}}{\Delta})^{\alpha}\right)\right)$, which is exponential with the subcarrier number but polynomial with other problem dimensions. This will be a very huge reduction in complexity if we select a fine value of Δ. Note that in the case of the non-linear models which ignore the frequency dependency, the complexity will be same as the above since the number of comparisons are unchanged.

D. Energy Harvesting in LoRaWAN

Low-Power Wide-Area Networking (LPWAN) technology offers long-range wireless connections for low data rate services. Among the existing protocols for LPWAN, LoRaWAN has captured interest in Industrial Internet of Things (IIoT) applications widely. In this example, we consider the same system as [33] but vary efficiency to highlight the impact of the non-linearity on the average battery life of a monitoring device, which is one of the major challenges. The battery life (in months) can be defined as

$$\mu(Life)_{batt.} = \frac{(Cap)_{batt.}}{30 \times (\mu(E)_{day} - \mu(E_h)_{day})}, \qquad (17)$$

where $(Cap)_{batt.}$ is the total battery capacity, $\mu(E)_{day}$ is the average energy consumed per day, and $\mu(E_h)_{day}$ is the amount of energy added to the battery from the energy harvesting per day. For simplicity, we assume the battery capacity is 1000 mAh (i.e., $11880J$@3.3 V). The average energy consumption of monitoring node per day against sensing intervals (1,2, and 3 min.) are taken from [33] as 85, 43, and 30 joules, respectively. For RF energy source, we assume a 3 W transmitted through 2 m distant source at 915 MHz, which has already been exploited by IIoT applications reported in [45], [46]. Fig. 7 compares the average battery life using the conventional constant efficiency model and our non-linear joint power and frequency dependent efficiency model against a range of reasonable sensing intervals. We assume the use of the harvester in [10]. As expected, the linear models considerably overestimate the average battery life, which results in a power outage of the field monitoring device.

VI. Conclusion

To the best of our knowledge, this paper has proposed, for the first time, a joint model that simultaneously models both the frequency and power dependency of the conversion efficiency. By leveraging practical energy harvesters available in the literature, we have provided several unified and mathematically tractable models that do not require knowledge of circuit parameters, for the energy harvester's conversion efficiency in wireless communication as a non-linear function of the frequency. After that, we have proposed Gaussian and Fourier models for Type-I and Type-II harvesters, respectively. Simulation results have shown the excellent match between the experimental data and the proposed models. Thence, a joint

model that utilises these models and the power dependency models of the conversion efficiency has proposed. From the application examples, we have shown that the non-linearity in the conversion efficiency has a significant impact on the communication systems' performance and design.

It is very interesting to discuss further the potential mitigation solutions of these non-linearities in the energy harvesting wireless communication. Such solutions will be very useful in improving the performances such as pre-distortion or compensation based on prediction.

REFERENCES

[1] A. Abrol and R. K. Jha, "Power optimization in 5G networks: A step towards GrEEn communication," *IEEE Access*, vol. 4, pp. 1355–1374, 2016.

[2] A. M. Siddiqui, L. Musavian, S. Aïssa, and Q. Ni, "Performance analysis of relaying systems with fixed and energy harvesting batteries," *IEEE Transactions on Communications*, vol. 66, no. 4, pp. 1386–1398, 2018.

[3] E. Boshkovska, D. W. K. Ng, N. Zlatanov, and R. Schober, "Practical non-linear energy harvesting model and resource allocation for SWIPT systems," *IEEE Communications Letters*, vol. 19, no. 12, pp. 2082–2085, Dec 2015.

[4] Y. Dong, M. J. Hossain, and J. Cheng, "Performance of wireless powered amplify and forward relaying over nakagami-*m* fading channels with nonlinear energy harvester," *IEEE Communications Letters*, vol. 20, no. 4, pp. 672–675, April 2016.

[5] Y. Chen, K. T. Sabnis, and R. A. Abd-Alhameed, "New formula for conversion efficiency of RF EH and its wireless applications," *IEEE Transactions on Vehicular Technology*, vol. 65, no. 11, pp. 9410–9414, Nov 2016.

[6] X. Xu, A. Özçelikkale, T. McKelvey, and M. Viberg, "Simultaneous information and power transfer under a non-linear RF energy harvesting model," in *2017 IEEE International Conference on Communications Workshops (ICC Workshops)*, May 2017, pp. 179–184.

[7] A. Georgiadis, G. V. Andia, and A. Collado, "Rectenna design and optimization using reciprocity theory and harmonic balance analysis for electromagnetic (EM) energy harvesting," *IEEE Antennas and Wireless Propagation Letters*, vol. 9, pp. 444–446, 2010.

[8] S. D. Assimonis, S. Daskalakis, and A. Bletsas, "Sensitive and efficient RF harvesting supply for batteryless backscatter sensor networks," *IEEE Transactions on Microwave Theory and Techniques*, vol. 64, no. 4, pp. 1327–1338, April 2016.

[9] H. Sun, Y. Guo, M. He, and Z. Zhong, "A dual-band rectenna using broadband Yagi antenna array for ambient RF power harvesting," *IEEE Antennas and Wireless Propagation Letters*, vol. 12, pp. 918–921, 2013.

[10] A. S. A. Y. Z. Miaowang Zeng, Zihong Li and H.-Z. Tan, "A compact dual-band rectenna for GSM900 and GSM1800 energy harvesting," *International Journal of Antennas and Propagation*, vol. 2018, p. 9 pages, 2018.

[11] Z. Du and X. Y. Zhang, "High-efficiency single- and dual-band rectifiers using a complex impedance compression network for wireless power transfer," *IEEE Transactions on Industrial Electronics*, vol. 65, no. 6, pp. 5012–5022, June 2018.

[12] A. M. Almohaimeed, M. E. E. Yagoub, J. A. Lima, and R. E. Amaya, "Dual-band harvester with wide range input power for WPT applications," in *2018 IEEE PELS Workshop on Emerging Technologies: Wireless Power Transfer (Wow)*, June 2018, pp. 1–4.

[13] A. Bakytbekov, T. Q. Nguyen, C. Huynh, K. N. Salama, and A. Shamim, "Fully printed 3D cube-shaped multiband fractal rectenna for ambient RF energy harvesting," *Nano Energy*, vol. 53, pp. 587 – 595, 2018. [Online]. Available: http://www.sciencedirect.com/science/article/pii/S2211285518306669

[14] C. Song, Y. Huang, P. Carter, J. Zhou, S. Yuan, Q. Xu, and M. Kod, "A novel six-band dual CP rectenna using improved impedance matching technique for ambient RF energy harvesting," *IEEE Transactions on Antennas and Propagation*, vol. 64, no. 7, pp. 3160–3171, July 2016.

[15] V. Palazzi, J. Hester, J. Bito, F. Alimenti, C. Kalialakis, A. Collado, P. Mezzanotte, A. Georgiadis, L. Roselli, and M. M. Tentzeris, "A novel ultra-lightweight multiband rectenna on paper for RF energy harvesting in the next generation LTE bands," *IEEE Transactions on Microwave Theory and Techniques*, vol. 66, no. 1, pp. 366–379, Jan 2018.

[16] M. M. Mansour and H. Kanaya, "Compact and broadband RF rectifier with 1.5 octave bandwidth based on a simple pair of L-section matching network," *IEEE Microwave and Wireless Components Letters*, vol. 28, no. 4, pp. 335–337, April 2018.

[17] C. Song, Y. Huang, J. Zhou, and P. Carter, "Improved ultrawideband rectennas using hybrid resistance compression technique," *IEEE Transactions on Antennas and Propagation*, vol. 65, no. 4, pp. 2057–2062, April 2017.

[18] Y. Shi, J. Jing, Y. Fan, L. Yang, J. Pang, and M. Wang, "Efficient RF energy harvest with a novel broadband Vivaldi rectenna," *Microwave and Optical Technology Letters*, vol. 60, no. 10, pp. 2420–2425, 2018. [Online]. Available: https://onlinelibrary.wiley.com/doi/abs/10.1002/mop.31362

[19] C. Song, Y. Huang, J. Zhou, J. Zhang, S. Yuan, and P. Carter, "A high-efficiency broadband rectenna for ambient wireless energy harvesting," *IEEE Transactions on Antennas and Propagation*, vol. 63, no. 8, pp. 3486–3495, Aug 2015.

[20] S. Wang, M. Xia, K. Huang, and Y. Wu, "Wirelessly powered two-way communication with nonlinear energy harvesting model: Rate regions under fixed and mobile relay," *IEEE Transactions on Wireless Communications*, vol. 16, no. 12, pp. 8190–8204, Dec 2017.

[21] P. N. Alevizos and A. Bletsas, "Sensitive and nonlinear far-field RF energy harvesting in wireless communications," *IEEE Transactions on Wireless Communications*, vol. 17, no. 6, pp. 3670–3685, June 2018.

[22] S. Wang, M. Xia, and Y. Wu, "Space-time signal optimization for swipt: Linear versus nonlinear energy harvesting model," *IEEE Communications Letters*, vol. 22, no. 2, pp. 408–411, 2018.

[23] S. Boyd and L. Vandenberghe, *Convex Optimization*. Cambridge University Press, 2004.

[24] A. M. Siddiqui, L. Musavian, S. Aïssa, and Q. Ni, "Weighted tradeoff between spectral efficiency and energy efficiency in energy harvesting systems," in *2019 IEEE 30th Annual International Symposium on Personal, Indoor and Mobile Radio Communications (PIMRC)*, 2019, pp. 1–6.

[25] H. Tran, G. Kaddoum, and K. T. Truong, "Resource allocation in swipt networks under a nonlinear energy harvesting model: Power efficiency, user fairness, and channel nonreciprocity," *IEEE Transactions on Vehicular Technology*, vol. 67, no. 9, pp. 8466–8480, 2018.

[26] Z. Wei, S. Sun, X. Zhu, D. In Kim, and D. W. K. Ng, "Resource allocation for wireless-powered full-duplex relaying systems with non-linear energy harvesting efficiency," *IEEE Transactions on Vehicular Technology*, vol. 68, no. 12, pp. 12 079–12 093, 2019.

[27] L. Jiang, B. Chen, S. Xie, S. Maharjan, and Y. Zhang, "Incentivizing resource cooperation for blockchain empowered wireless power transfer in uav networks," *IEEE Transactions on Vehicular Technology*, vol. 69, no. 12, pp. 15 828–15 841, 2020.

[28] L. Jiang, S. Xie, S. Maharjan, and Y. Zhang, "Blockchain empowered wireless power transfer for green and secure internet of things," *IEEE Network*, vol. 33, no. 6, pp. 164–171, 2019.

[29] H. Tran and G. Kaddoum, "Robust design of ac computing-enabled receiver architecture for swipt networks," *IEEE Wireless Communications Letters*, vol. 8, no. 3, pp. 801–804, 2019.

[30] S. Shen and B. Clerckx, "Beamforming optimization for mimo wireless power transfer with nonlinear energy harvesting: Rf combining versus dc combining," *IEEE Transactions on Wireless Communications*, pp. 1–1, 2020.

[31] K. Huang and E. Larsson, "Simultaneous information and power transfer for broadband wireless systems," *IEEE Transactions on Signal Processing*, vol. 61, no. 23, pp. 5972–5986, Dec 2013.

[32] H. Kim, H. Lee, M. Ahn, H. Kong, and I. Lee, "Joint subcarrier and power allocation methods in full duplex wireless powered communication networks for OFDM systems," *IEEE Transactions on Wireless Communications*, vol. 15, no. 7, pp. 4745–4753, July 2016.

[33] H. H. R. Sherazi, L. A. Grieco, M. A. Imran, and G. Boggia, "Energy-efficient lorawan for industry 4.0 applications," *IEEE Transactions on Industrial Informatics*, vol. 17, no. 2, pp. 891–902, 2021.

[34] S. Kim, H. Abbasizadeh, B. S. Rikan, S. J. Oh, B. G. Jang, Y. Park, D. Khan, T. T. K. Nga, K. T. Kang, Y. G. Pu, S. Yoo, S. Lee, S. Lee, M. Lee, K. C. Hwang, Y. Yang, and K. Lee, "A -20 to 30 dbm input power range wireless power system with a mppt-based reconfigurable 48efficient rf energy harvester and 82with open-loop delay compensation," *IEEE Transactions on Power Electronics*, vol. 34, no. 7, pp. 6803–6817, 2019.

[35] P. H. Moose, "A technique for orthogonal frequency division multiplexing frequency offset correction," *IEEE Transactions on Communications*, vol. 42, no. 10, pp. 2908–2914, 1994.

[36] H. Motulsky and A. Christopoulos, *Fitting Models to Biological Data Using Linear and Nonlinear Regression: A Practical Guide to Curve Fitting*. Oxford University Press, 2004. [Online]. Available: https://books.google.co.uk/books?id=tIsjh56pI0IC
[37] S. Corovic, I. Lackovic, P. Sustaric, T. Sustar, T. Rodic, and D. Miklavcic, "Modeling of electric field distribution in tissues during electroporation," *BioMedical Engineering OnLine*, vol. 12, no. 1, p. 16, Feb 2013. [Online]. Available: https://doi.org/10.1186/1475-925X-12-16
[38] H. Tafekirt, J. Pelegri-Sebastia, A. Bouajaj, and B. M. Reda, "A sensitive triple-band rectifier for energy harvesting applications," *IEEE Access*, vol. 8, pp. 73 659–73 664, 2020.
[39] C. Song, A. López-Yela, Y. Huang, D. Segovia-Vargas, Y. Zhuang, Y. Wang, and J. Zhou, "A novel quartz clock with integrated wireless energy harvesting and sensing functions," *IEEE Transactions on Industrial Electronics*, vol. 66, no. 5, pp. 4042–4053, 2019.
[40] C. Song, Y. Huang, J. Zhou, P. Carter, S. Yuan, Q. Xu, and Z. Fei, "Matching network elimination in broadband rectennas for high-efficiency wireless power transfer and energy harvesting," *IEEE Transactions on Industrial Electronics*, vol. 64, no. 5, pp. 3950–3961, May 2017.
[41] K. Niotaki, S. Kim, S. Jeong, A. Collado, A. Georgiadis, and M. M. Tentzeris, "A compact dual-band rectenna using slot-loaded dual band folded dipole antenna," *IEEE Antennas and Wireless Propagation Letters*, vol. 12, pp. 1634–1637, 2013.
[42] Y. Shi, Y. Fan, Y. Li, L. Yang, and M. Wang, "An efficient broadband slotted rectenna for wireless power transfer at lte band," *IEEE Transactions on Antennas and Propagation*, vol. 67, no. 2, pp. 814–822, 2019.
[43] J. Shi, W. Yu, Q. Ni, W. Liang, Z. Li, and P. Xiao, "Energy efficient resource allocation in hybrid non-orthogonal multiple access systems," *IEEE Transactions on Communications*, vol. 67, no. 5, pp. 3496–3511, 2019.
[44] M. Grant, "Cvx: Matlab software for disciplined convex programming." [Online]. Available: http://cvxr.com/cvx
[45] F. Touati, A. Galli, D. Crescini, P. Crescini, and A. B. Mnaouer, "Feasibility of air quality monitoring systems based on environmental energy harvesting," in *2015 IEEE International Instrumentation and Measurement Technology Conference (I2MTC) Proceedings*, 2015, pp. 266–271.
[46] X. Lu, P. Wang, D. Niyato, D. I. Kim, and Z. Han, "Wireless networks with RF energy harvesting: A contemporary survey," *IEEE Communications Surveys Tutorials*, vol. 17, no. 2, pp. 757–789, Secondquarter 2015.

Dokhyl AlQahtani (S'15) received the B.Sc. and M.Sc. degrees in electrical engineering from King Saud University, Riyadh, Saudi Arabia, in 2010, and 2015, respectively. He served as a Lecturer with the Electrical Engineering Department, College of Engineering, Prince Sattam bin Abdulaziz University, Al-Kharj, Saudi Arabia, before joining the University of Warwick, U.K, where he is currently pursuing the Ph.D. degree with the School of Engineering. His research interest is currently focused on the performance evaluation, optimization, and design of energy harvesting-based communication systems.

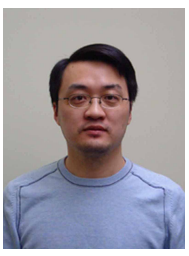

Yunfei Chen (S'02-M'06-SM'10) received his B.E. and M.E. degrees in electronics engineering from Shanghai Jiaotong University, Shanghai, P.R.China, in 1998 and 2001, respectively. He received his Ph.D. degree from the University of Alberta in 2006. He is currently working as an Associate Professor at the University of Warwick, U.K. His research interests include wireless communications, cognitive radios, wireless relaying and energy harvesting.

Wei Feng (Senior Member, IEEE) received the B.S. and Ph.D. degrees from the Department of Electronic Engineering, Tsinghua University, Beijing, China, in 2005 and 2010, respectively. He is currently an Associate Professor with the Department of Electronic Engineering, Tsinghua University. His research interests include maritime communication networks, large-scale distributed antenna systems, and coordinated satellite-UAV-terrestrial networks. He serves as the Assistant to the Editor-in-Chief of China Communications, and an Editor of IEEE Transactions on Cognitive Communications and Networking.

Mohamed-Slim Alouini (S'94-M'98-SM'03-F'09) was born in Tunis, Tunisia. He received the Ph.D. degree in Electrical Engineering from the California Institute of Technology (Caltech), Pasadena, CA, USA, in 1998. He served as a faculty member in the University of Minnesota, Minneapolis, MN, USA, then in the Texas A&M University at Qatar, Education City, Doha, Qatar before joining King Abdullah University of Science and Technology (KAUST), Thuwal, Makkah Province, Saudi Arabia as a Professor of Electrical Engineering in 2009. His current research interests include modeling, design, and performance analysis of wireless communication systems.